energies

MDPI

Article

Investigation of an Inclined Heat Pipe Heat Exchanger as a Passive Cooling Mechanism on a Photovoltaic Panel

Samiya Aamir Al-Mabsali [1], Jay Pillo Candido [2], Hassam Nasarullah Chaudhry [3,*] and Mehreen Saleem Gul [1]

[1] School of Energy, Geoscience, Infrastructure and Society, Heriot-Watt University, Edinburgh EH14 4AS, UK; saa83@hw.ac.uk (S.A.A.-M.); M.Gul@hw.ac.uk (M.S.G.)
[2] Department of Engineering, University of Technology and Applied Sciences, Muscat P.O. Box 74, Oman; jay.candido@hct.edu.om
[3] School of Energy, Geoscience, Infrastructure and Society, Heriot-Watt University Dubai Campus, Heriot-Watt University, Dubai Knowledge Park, Dubai P.O. Box 38103, United Arab Emirates
* Correspondence: h.n.chaudhry@hw.ac.uk

Abstract: An investigation on the heat transfer coefficient (HTC) of a heat pipe heat exchanger (HPHE) was carried out while being installed as a cooling mechanism on photovoltaic panels. The Ecohouse at the University of Technology and Applied Sciences in Muscat, Oman, was used as the case study. The experiment monitored the effect of temperature variations on PV-HPHE-induced power generation. The heat pipes were arranged in a double-sided condenser in a spanwise manner with spacing 50 mm in the center with an inclination angle of 3°. J-type thermocouples (exposed wire, polytetrafluoroethylene (PTFE) insulated) with a tip diameter of 1.5 mm were used. The results indicated mean values of HTC that were measured at 2.346 W/m^2 K. The findings showed that the HTC values possessed a minimal standard error from the effect of variations of the ambient temperature. The mean HTC value of 2.346 W/m^2 K can be used in the succeeding experiments using the same novel PV-HPHE setup. Additional results showed the recorded variations from the mean value of the HTC effect on the HPHE heat flow generation, which resulted in a 29% increase in power performance efficiency using PV-HPHE.

Keywords: heat transfer coefficient; heat pipe; photovoltaic

Citation: Aamir Al-Mabsali, S.; Candido, J.P.; Chaudhry, H.N.; Gul, M.S. Investigation of an Inclined Heat Pipe Heat Exchanger as a Passive Cooling Mechanism on a Photovoltaic Panel. *Energies* **2021**, *14*, 7828. https://doi.org/10.3390/en14237828

Academic Editor: Dmitry Eskin

Received: 19 October 2021
Accepted: 18 November 2021
Published: 23 November 2021

1. Introduction

The Sultanate of Oman has a strong commitment to the promotion of an eco-friendly lifestyle with the creation of a greener future for generations to come. The government of Oman created an initiative to generate energy from renewable resources with a long-term program that started in 2008. Furthermore, the country aims to reduce the reliance on local fossil fuel energy resources, as well as produce a surplus of power that can be shared for the benefit of its citizens [1]. The current study was conducted in the Ecohouse research facility in Oman and aimed to provide a solution to the low power capacity due to the exposure of photovoltaic (PV) panels to the very high ambient temperatures that are experienced in the region. This study is a continuation of Al Mabsali et al.'s [2] experimental investigation, which specified the optimal heat pipe heat exchanger (HPHE) arrangement and installation that can restore the loss in PV performance efficiency and increase power production, as shown in Figure 1.

Table 2019 reached 33.8 TWh, 0.7% higher than in 2018, which was 32.5 TWh and the 2018 supply was 3.7% higher than in 2017 based on the APSR in 2018 [3] and 2019 [4]. In addition to energy management strategies, renewable-energy-driven technologies are the most viable alternatives as solutions to meet the increasing energy demand of the Sultanate. Among these technologies, solar photovoltaics (PVs) are the most promising technology due to the strong support from the Omani government. The APSR, [1] developed a

government regulatory focus program called the SAHIM initiative for small-scale grid-connected solar PV systems. SAHIM, which means 'contribute' in Arabic, introduced rooftop solar panels to buildings across the country and aimed to generate sustainable and affordable clean energy. The objectives of SAHIM were to promote renewable energy in Oman through the deployment of a clean, sustainable and efficient PV technology on residential and other premises; to promote demand reduction, particularly at times of system peak demand; and thereby reduce quantities of electricity supplied from the main interconnected system that is sourced from the centrally dispatched gas plant to promote distributed generation and thereby reduce the magnitude and cost of transmission and distribution system losses and to deliver long-term reductions in electricity subsidies. However, extreme climates, such as that of Oman, present challenges in terms of exposure of the PV panels to high cell temperatures, which result in performance deterioration.

Figure 1. PV-HPHE apparatus isometric model (**left**) and captured infrared image (**right**) that were taken from the bottom surface in the Ecohouse, UTAS (formerly HCT), Muscat, Oman.

Al Mabsali et al. [5] conducted an experiment on the panel efficiency of PVs that were installed on the Ecohouse, UTAS, to conclude that the actual power production was inversely proportional to the PV cell temperature when it reached 83.65 °C. This indicated that the efficiency of the PV panels decreased from its rated power output when exposed to higher temperatures. In order to restore the PV panel efficiency and the study proposed to install heat pipe heat exchangers (HPHE) as a passive cooling mechanism. The major finding of the study indicated that the 50 mm HPHE spacing (2.5D, i.e., 2.5 times the diameter of the pipe) had the greatest potential to decrease the panel temperature, with a reduction of 9 °C in the NOCT from 64.5 °C (337.65 K) down to 55.32 °C (328.47 K). The recommended HPHE design installation was made of a double-sided condenser with a middle section installation that had a 90° spanwise orientation towards the PV panel. The experimental testing indicated a temperature drop between the heat pipe and the duct section. The maximum internal temperature of 52.43 °C and minimum internal temperature of 45.61 °C were obtained in the heat pipe section containing water. A temperature of 54 °C was read in the duct section, which was greater than the numerically predicted results in the heat pipes.

Heat transfer in inclined pipes has a very wide range of heat exchanger applications in the industry, one of which is in solar energy collectors. The heat transfer coefficient is defined by the relation of an equation to be proportional to the rate of heat flow affecting similar or different phases of matter. The heat transfer coefficient is inversely proportional to the product of the area over which the heat transfer occurs and the characteristic temperature difference. The heat transfer coefficient has been used in modelling convective heat transfer since the time of Newton in the 18th century. This coefficient is usually determined experimentally and no well-found theoretical approach was available until the last few decades [6]. The HPHE natural convection flow velocities are small and may be negligible. However, in electronics and PV applications, it may be the only relevant mechanism of heat transfer to use in passive cooling.

Churchill and Chu [7] equated the product of the heat transfer coefficient and the length of material to the product of the thermal conductivity of the material and the Nusselt number. The establishment of the HTC of the HPHE simplified the determination of the Nusselt number in the follow-up experiments to be made. The Nusselt number is used to determine the fluid flow in pipes: it is a fully developed laminar flow when less than 4.364 for constant heat flux and 3.66 for uniform wall temperature.

Natural Convective Heat Transfer Coefficient in Inclined Heat Pipes

Chaudhry et al. [8] reviewed standard tubular heat pipe systems, which presented the largest operating temperature range in comparison with other heat pipes and offered viable potential for optimisation and integration into renewable energy systems, such as solar PV. This efficient performance may be affected by the behaviour of convective heat transfer, especially in inclined heat pipes. An inclination effect on heat transfer coefficients during convective condensation was first noticed by Chato [9]. For downwards flows in slightly inclined tubes, raising the inclination increased the heat transfer coefficient because of the subsidence of the liquid depth in the tube. Mosyak and Hetsroni [10] also measured the temperature difference between the top and bottom of a horizontal pipe and slightly inclined pipes and found that increasing the pipe inclination could drastically reduce the temperature difference.

Hetsroni et al. [11] investigated the local heat transfer coefficient of upwards air–water flow in inclined pipes and claimed that the pipe inclination enhanced the two-phase heat transfer. Gualos et al. [12] conducted experimental tests on a thermosyphon loop using water as the working fluid. A two-phase loop consisting only of a condenser and an evaporator separated by the liquid and vapour lines was developed. It used the concept of phase change to transfer energy from the heat source to the condenser. Evaporation and condensation heat transfer coefficients were measured under variations in the heat load. G. N. Kruzhilin [13] proposed a new empirical correlation for evaporation heat transfer in the thermosyphon based on the Cooper correlation, resulting in a mean deviation of 10%. In the condenser section, the experimental measurements followed Wang et al.'s [14] correlation trend. A simple modification of the correlation of Koyama et al. [15] showed excellent quantitative agreement with the current study's experimental measurements. The results showed that the evaporator thermal resistance could be reduced by up to 75% compared with a smooth surface evaporator at low heat flux. In the same condition, the system thermal resistance could be diminished by up to 20%.

Y. Mori et al.'s [16] study of laminar heat transfer in horizontal circular tubes with a constant heat flux boundary condition was extensively investigated in the past, especially between the 1950s and 1990s. They found that as the density of almost all fluids was dependent on temperature, the addition of heat to the tube wall led to mixed convection due to the temperature gradients inside the thermal boundary layer, which resulted in density differences and buoyancy effects in the presence of gravity. Mohammed et al. [17] paid more attention to the effect of free convection on laminar heat transfer coefficients, especially when the flow was fully developed. The effect of free convection not only increased the heat transfer and pressure drop but also reduced the thermal entrance lengths and induced an early transition to turbulent flow.

Papoutsakis et al. [18] presented an analytical solution for a uniform heat flux over a segment of a duct wall, together with a uniform temperature that was far upstream of the heated section. The approach did not address the arbitrary inlet temperature profiles. Upon its application, due to the finiteness of the wall's thermal conductivity, the wall heat flux density was never discontinuous.

Colle [19] partially solved this problem by extending the solution to cover what he called 'arbitrary' boundary conditions, However, this was still limited to cases where temperature asymptotically behaved like uniform values both upstream and downstream. Warrington and Powe [20] conducted an experiment on natural convection heat transfer between concentrically located isothermal spherical, cylindrical and cubical inner bodies

and their isothermal cubical enclosure. The results highlighted that the enclosure shape has only a small effect on the temperature profile and heat transfer results, which never exceeded 3.1%. However, the enclosure length-over-radius ratio applied in the every Nusselt number equation had a significant effects of 13.51 to 18.5% average deviations based on the results. The many different flow patterns and temperature profiles, whether unsteady or not, had very little effect on the overall heat transfer.

The basic principle of fluid viscosity in the calculation of heat transfer coefficient is affected by two major factors, which are the cohesive forces and the molecular momentum transfer, both of which are temperature-dependent. In fluids, an increase in the bulk temperature will cause the viscosity to decrease and can create a significant variation in the heat transfer coefficient values. L. Wang et al. [21] conducted work on the effects of temperature-dependent viscosity on the natural convection in a porous cavity with a circular cylinder under local thermal non-equilibrium (LTNE) conditions. The numerical results showed that the LTNE parameters of the inter-phase heat transfer coefficient on flow and the ratio of fluid-to-solid thermal conductivity increased. The absolute and kinematic viscosities of the fluid are important in the specific applications of the dimensionless numbers that are required in the determination of the value of the heat transfer coefficient.

Nakai and Okazaki [22] investigated the heat transfer from a horizontal wire cylinder using mixed, forced and free convection. Theoretical correlations at small Reynolds and Grashof numbers were given using the expansion method, similar to the cases of pure convection. The effects of the slight convection on the heat transfer were expressed systematically using a parameter in terms of Nusselt, Reynolds, Grashof and Prandtl numbers.

Forsberg [23] used three major dimensionless numbers, namely, the Nusselt, Reynolds and Prandtl numbers, to associate basic considerations that are required for forced convection models. For natural convection, the fluid flow was caused by density gradients in the fluid. Therefore, the Reynolds number has no relevance and can be replaced by the Grashof number with the difference between the surface and bulk liquid temperatures as an absolute value. Furthermore, as adopted in this study, the free convection experimental data were correlated using the Grashof, Prandtl and Nusselt numbers. Another dimensionless number that is found in natural convection correlations was the Rayleigh number, which is the product of the Grashof and Prandtl numbers. The Prandtl number is used to specify the steady phase of a refrigerant that is exposed to temperature variations. The local convective heat transfer coefficient can be calculated accurately using the Nusselt number. The Nusselt number is the ratio of convective to conductive heat transfer at a boundary in a fluid and is also used to determine fluid flow in pipes. Conduction heat transfer is greater than convection heat transfer when the value of the Nusselt number is less than 1. This result is an indication that the liquid phase of water is stable and has not transformed to vapour during the heat transfer process.

2. Mathematical Principles

This section explains the mathematical equations that were used in the determination of the mean value of the natural heat transfer coefficient to be applied in the heat flow calculation of the HPHE. The HTC was also determined from the experimental set-up as an empirical value that is exclusive to the novel PV-HPHE apparatus under investigation. The results were utilised to ascertain the PV-HPHE power performance with respect to the effects of various temperatures observed using the Thermocouples, Picolog and Watchpower software.

2.1. Governing Equations—Newton's Law of Cooling

Davidzon [24] theory and practice of heat transfer mechanisms calculations were often directed to a value called the 'heat transfer coefficient', which is experimentally defined from Newton's law of cooling (Equation (1)), along with Fourier's law. The intensity of energy transfer in the form of heat depends on the difference in the temperatures of the

interacting physical systems, which was a generalisation of experiments by Newton. Using Equation (1) in the calculation of convective heat transfer concluded that this was probably not Newton's law in general, but a kind of expression that can be supported by experiments under some conditions, but not under others. Their study recommended that an actual observation of the heat transfer coefficient should be determined in every experimental setup. Citing the physics of the phenomenon of heat exchange, further development of the existing equations from models is necessary, or the creation of new, more adequate equations from models is required.

$$Q = h\ A\ (T_W - T_\infty) \tag{1}$$

$$Q = h\ A\ \Delta T_{lm} \tag{2}$$

where Q—heat transferred per unit time or heat flow (W), h—empirical value of the overall heat transfer coefficient ($W/m^2\ ^\circ C$), A—heat transfer area (m^2), T_W—temperature of the heating surface (wall temperature (°C)); T_∞—ambient temperature (°C). In relation to Equations (1) and (2), q = Q/A is the heat flux (W/m^2).

2.2. Temperature-Dependent Property Data

Calculations of the temperature variations due to convection were compared using Chatterjee et al.'s [25] mean theoretical bulk liquid temperature T_b. In this study, the bulk temperature was calculated from the mean values of the evaporator and condenser sections inlet liquid temperatures. The data were taken from 10:00 a.m. to 2:00 p.m. when the liquid flow was thermally fully developed.

$$T_b = \frac{T_{con,in} + T_{evap,in}}{2} \tag{3}$$

R. Sinnott and G. Towler's [26] basic design procedure and theory presented the general equation for the temperature driving force that is applied in a shell and tube heat exchanger. This equation was used to calculate the mean temperature difference ΔT_m and could be estimated by applying a correction factor Ft to the logarithmic mean temperature.

$$\Delta T_m = F_t\ \Delta T_{lm} \tag{4}$$

$$\Delta T_{lm} = \frac{(T_1 - t_2) - (T_2 - t_1)}{\ln \frac{(T_1 - t_2)}{(T_2 - t_1)}} \tag{5}$$

$$R = \frac{(T_1 - T_2)}{(t_2 - t_1)} \tag{6}$$

$$S = \frac{(t_2 - t_1)}{(T_1 - t_1)} \tag{7}$$

$$F_t = \frac{\sqrt{\left(R^2 + 1\right)} 1n\left[\frac{(1-S)}{(1-RS)}\right]}{(R-1) 1n\left[\frac{2-S\left[R+1-\sqrt{\left(R^2+1\right)}\right]}{2-S\left[R+1+\sqrt{\left(R^2+1\right)}\right]}\right]} \tag{8}$$

where ΔT_m—log mean temperature. T_1—hot fluid inlet temperature, T_2—hot fluid outlet temperature, t_1—cold fluid inlet temperature and t_2—cold fluid inlet temperature. R and S are dimensionless temperature ratios and not considered in this study. This is because R is equal to the shell-side fluid flow rate times the fluid mean specific heat divided by the tube-side fluid flow rate times the tube-side fluid specific heat. S is a measure of the temperature efficiency of the exchanger. For a one-shell, two-tube pass exchanger, the PV-HPHE apparatus has no tubes installed and this will result in $t_1 = 0$ and $t_2 = 0$. When $t_1 = 0$ and $t_2 = 0$, then $F_t = -1$.

According to R. Sinnott and G. Towler [26], utilising Equation (8) is the same for co-current flow, but the terminal temperature differences will be ($T_1 - t_1$) and ($T_2 - t_2$). The application of Equation (8) was based on the following conditions: when there is no change in the specific heats, the overall heat transfer coefficient is constant, and there are no heat losses. In a design, these conditions can be assumed to be satisfied, provided that the temperature change in each fluid stream is not large. The characteristics of Equation (8) are almost compatible with the function of the HPHE in this study.

The determination of the properties of water that were required in this study is specified in this section. The thermal conductivity k, heat capacity Cp, density ρ and dynamic viscosity μ were calculated based on temperature-dependent polynomials at constant pressure with temperature increments. The polynomials cited from [27] are listed below in Equations (9)–(12).

$$\rho = 1001.3 - 0.155T_b - 2.658 \times 10^{-3}T_b^2 \quad (9)$$

$$\log_{10}\mu = -2.750 - 0.0141T_b + 91.9 \times 10^{-6}T_b^2 - 311 \times 10^{-9}T_b^3 \quad (10)$$

$$cp = 4209 - 1.31T_b + 0.014T_b^2 \quad (11)$$

$$k = 0.5706 + 1.756 \times 10^{-3}T_b - 6.46 \times 10^{-6}T_b^2 \quad (12)$$

A correlation under laminar flow using dimensionless numbers was determined to predict the effect of the power capacity efficiency of an inclined partially filled HPHE that was exposed to passive cooling. The dimensionless numbers that were taken from [7] that were used in the determination of the empirical equation of the convective heat transfer coefficient were as follows:

Prandtl number

$$Pr = \frac{cp\,\mu}{k} \quad (13)$$

Grashof number

$$Gr = \frac{g\ \beta\ (T_s - T_\infty)\ L^3}{v^2} \quad (14)$$

Reynolds number

$$Re_f = \frac{\dot{Q}\rho}{\mu D} \quad (15)$$

Rayleigh number

$$\frac{g\ \beta\ (T_s - T_b)\ D^3}{v\alpha} \quad (16)$$

Nusselt number

$$Nu = 0.36 + 0.518\left(\frac{Ra}{\left[1+\left(\frac{0.559}{Pr}\right)^{\frac{9}{16}}\right]^{\frac{16}{9}}}\right)^{\frac{1}{4}} \quad (17)$$

2.3. Data Reduction

According to Chaudhry et al.'s [28] experimental determination of the thermal performance of the heat pipe heat exchanger, it is required that the temperatures that are taken from the phase refrigerant be precise. The accuracy of measurements from different locations of the heat exchanger to determine the rate of heat transfer across its length must be specified. The characterisation of the evaporator section was carried out by averaging the temperature measurements at the respective locations at regular time intervals. The density and specific heat capacity values were taken in accordance with the source temperatures. The rate of heat transfer in the evaporator section was formulated using Equation (18).

$$q'' = \frac{\dot{m}\,C_p\,(T_b)}{A_{surface}} \quad (18)$$

Quantification of the thermal performance of the heat pipes was based on the concept of heat exchanger effectiveness. The effectiveness of a heat exchanger is the ratio of the actual rate of heat transfer by the heat exchanger to the maximum possible heat transfer rate between the phase materials, as formulated in Equation (19).

$$\varepsilon = \frac{q_{actual}}{q_{max}} = \frac{T_{e,inlet} - T_{e,outlet}}{T_{e,inlet} - T_{c,inlet}} \tag{19}$$

Chatterjee et al. [25] applied the Buckingham Pi theorem regarding liquid properties on a dimensioned surface area, given in Equation (20), to determine the heat flux based on the temperature-dependent polynomial that was cited by the National Institute of Standards and Technology [29]. Churchill and Chu's [7] convective heat transfer coefficient was used and is shown in Equation (21).

$$A_{surface} = \pi DL \tag{20}$$

$$h = \frac{k}{L}Nu \tag{21}$$

where q" is the heat flux that is transferred to the liquid in the HPHE. The fluid properties, such as heat capacity Cp, coefficient of thermal conductivity k, density ρ and dynamic viscosity μ in Equations (9)–(12), were calculated at the average bulk temperature, i.e., Tb, as given by Equation (3). The heat transfer area was a surface and was calculated as given in Equation (20).

The heat flow Q in watts (W) could be derived from the equation used in the determination of the PV and PV-HPHE power generation and the experimental data that was produced on site. The difference in the power generation between the PV panel and PV-HPHE from the data in the Watchpower software was used in the determination of the power performance of HPHE, as shown in Equation (22). The mean value of the HPHE efficiency was established using the data taken from 2 to 14 August 2020. The HPHE efficiency is the ratio of its power performance relative to the PV panel power generation, as shown in Equation (23).

Because of the limitation in the number of thermocouples in the Picolog, no data of the PV panel power generation was taken from the period of 14–21 September 2020. By using Equations (22) and (23), the PV panel generation could be determined using Equation (24). This could be achieved by substituting the established mean value of the HPHE efficiency and the PV-HPHE power generation data taken from 14 to 21 September 2020.

The theoretical equation of the HPHE power generation was formulated and could be equated to its theoretical heat flow Q, as shown in Equation (25). This could be determined with the use of the established mean value of the HPHE efficiency and any provided data from the power generation of the PV-HPHE.

$$P_{HPHE} = P_{PV-HPHE} - P_{PV} \tag{22}$$

$$\text{Efficiency} = \frac{(P_{PV-HPHE} - P_{PV})}{P_{PV}} \tag{23}$$

$$\text{Efficiency} = \left(\frac{P_{PV-HPHE}}{P_{PV}}\right) - \left(\frac{P_{PV}}{P_{PV}}\right)$$

$$P_{PV-HPHE} = (\text{Efficiency} + 1)P_{PV}$$

$$P_{PV} = \frac{P_{PV-HPHE}}{\text{Efficiency} + 1} \tag{24}$$

$$P_{HPHE} = \frac{P_{PV-HPHE} - P_{PV-HPHE}}{(\text{Efficiency} + 1)}$$

$$P_{HPHE} = P_{PV-HPHE}\left[1 - \frac{1}{(\text{Efficiency} + 1)}\right]$$

$$P_{HPHE} = P_{PV-HPHE}\left[\frac{(Efficiency + 1) - 1}{(Efficiency + 1)}\right]$$
$$P_{HPHE} = Q = P_{PV-HPHE}\left[\frac{Efficiency}{(Efficiency + 1)}\right] \quad (25)$$

3. Experimental Methodology

Two similar PV panels were used in the experiment. The first PV panel was used to set a baseline model and provide independent data of power performance. The second PV panel incorporated the HPHE and was used to obtain the panel temperature variations and the effect on PV power production. The PV panel specifications were the following: 1956 × 992 × 6 mm^3 surface dimensions, polycrystalline silicone PV module with a maximum power of 300 WVMP and 36 V. R. G. Ross's [30] approximation equation was used to calculate the PV cell temperature:

$$T_{Cell} = T_{ambient} + \frac{(NOCT - 20) \times S}{800} \quad (26)$$

where T_{Cell}—PV surface cell temperature; T_∞—ambient temperature; NOCT is the PV nominal operating cell temperature; and S is the solar irradiation, which is equal to 911.11 W/m^2 (Al Mabsali et al) [2].

In order to monitor the effect of temperature variations on PV power generation, thermocouples were installed at seven locations of the apparatus. The first sensor was installed to determine the ambient temperature and two sensors were attached to the PVs' top and bottom surfaces. Four sensors were installed in the heat pipes in which two sensors were on the external surface of the evaporator and condenser. Another two sensors were placed to determine the bulk temperature of the evaporator and condenser sections' inlet liquid temperatures. The total computational domain was split and refined at two specific surfaces, namely, the heat pipe external wall and the internal zone where the liquid is located. The data observations were taken from 14 to 21 September 2020 as the basis of the relationship of the variables under investigation.

3.1. Boundary Conditions and Solution Techniques

The PV-HPHE boundary conditions vary with the different working conditions. The fraction of the absorbed solar radiation as heat input in accordance with the PV panel surface temperature was considered as the PV electrical power generation. The decrease in PV-HPHE efficiency is affected by the increased temperature of the PV panel and the natural convection heat transfer of the bulk liquid that is absorbed by the heat pipes, which contributes an important part regarding the temperature reduction of the PV panels.

The temperature-dependent properties of the working fluid that is used within the heat pipes were accurately determined. The range of fluid density and dynamic viscosity values are tabulated in Table 1. The refrigerant thermal performance with increasing temperatures due to the convection heat transfer was investigated. The applied boundary conditions on the heat exchanger computational domain comprised a specific heat capacity with an initial temperature of 20 °C and was computed using linear interpolation as the mean bulk temperature increased.

The total cross-sectional area of the test section was 0.561 m^2 and the evaporator-to-condenser length was 0.248 m, indicating a negligibly low mean Reynolds number < 5. This dimensionless number was replaced by the Grashof number, which was proven applicable to natural convection heat transfer under laminar flow. Churchill and Chu's [7] theoretical and experimental equation was specified to analyse the temperature in order to achieve a direct comparison with the obtained results. The laminar regime boundary layer theory was utilised to derive numerical solutions for cylinders exposed to convective heat transfer. Saville and Churchill [31] showed that these solutions are quite accurate for moderate Rayleigh numbers where the wake was confined to a small region at the rear of the cylinder. For the asymptotic cases of Pr approaching ∞ and 0, [32] and [31], respectively, derived

solutions for the mean Nusselt number. The boundary conditions of the HPHE empirical heat transfer coefficient were investigated by using the mean outdoor temperature values that were observed during the testing period of 14–21 September 2020.

Table 1. Temperature-dependent properties of water.

Date	Mean Bulk Temp	Bulk Temp Diff.	Local Thermal Conductivity	Heat Capacity	Fluid Density	Fluid Viscosity	Thermal Diffusivity	Kinematic Viscosity	Coeff. of Thermal Expansion
	Tb (°C)	ΔT (°C)	k (W/m °C)	Cp (J/(kg °C))	ρ (kg/m^3)	μ (N s/m^2)	$\alpha = k/\rho C_p$ (m^2/s)	$\nu = \mu/\rho$ (m^2/s)	β (210^{-6}/20 °C)
14/09/20	33.21	8.96	0.622	4180.934	992.22	7.44×10^{-4}	1.50×10^{-7}	7.50×10^{-7}	3.49×10^{-4}
16/09/20	32.63	9.14	0.621	4181.162	992.41	7.53×10^{-4}	1.50×10^{-7}	7.59×10^{-7}	3.43×10^{-4}
17/09/20	32.91	9.17	0.621	4181.050	992.32	7.49×10^{-4}	1.50×10^{-7}	7.55×10^{-7}	3.46×10^{-4}
18/09/20	32.30	9.24	0.621	4181.292	992.52	7.58×10^{-4}	1.50×10^{-7}	7.64×10^{-7}	3.39×10^{-4}
19/09/20	32.32	9.35	0.621	4181.286	992.51	7.58×10^{-4}	1.50×10^{-7}	7.64×10^{-7}	3.39×10^{-4}
20/09/20	33.61	9.34	0.622	4180.786	992.09	7.38×10^{-4}	1.50×10^{-7}	7.44×10^{-7}	3.53×10^{-4}
21/09/20	34.98	9.20	0.624	4180.307	991.63	7.18×10^{-4}	1.51×10^{-7}	7.24×10^{-7}	3.67×10^{-4}

3.2. Experimental Set Up

The experiment was carried out on site. A heat pipe heat exchanger (HPHE) was installed below the PV panel, as shown in Figures 1 and 2. The HPHE and PV panel temperature measurements were monitored during the same period. Two theoretical temperature equations that were cited from related studies were used to compare the data taken from the experimental results. The first equation was the mean theoretical bulk liquid temperature that was used by Chatterjee et al. [25]. The second equation was the mean temperature difference general equation for the temperature driving force. This equation was applied by R. Sinnott and G. Towler [26] in a shell and tube heat exchanger for the purpose of validation.

The HPHE middle section was used for testing and carrying out the experimentation. The setup comprised of 40 pcs–20 mm diameter cylindrical copper heat pipes with a length of 492 mm, which were inserted on a 496 × 1959 × 30 mm^3 rectangular aluminum duct. The heat pipes were arranged in a double-sided condenser direction that was spanwise with a spacing of 50 mm in the centers with an inclination angle of 3°.

Alammar et al. [33] investigated the effect of the inlet temperature of the cooling water. The results showed that a fill ratio of 65% caused the period to increase with increasing inlet temperature for all four angles. This was also true for fill ratios of 25 and 100% at the angle of 10° only. The results for the remaining angles of 90, 60 and 30° and fill ratios of 25 and 100% had period decreases as the inlet temperature increased. In addition, for fill ratios of 25 and 100%, a small period was obtained at angles of 90 and 60° and inlet temperatures of 20 and 25 °C. The result was consistent for the fill ratio of 100% at an angle of 30°. Chatterjee et al. [25] presented an experimental investigation of single-phase heat transfer characteristics in a partially filled inclined rotating heated pipe with continuous axial liquid flow. The flow rate range of 100–830 mL/min and rotation rate range of 10–300 revolutions per minute were investigated by adopting various inclination angles from 0 to 6°. The wall heat flux (1405–10,784 W/m^2) was varied within the bounds of the single-phase flow operation. The local heat transfer coefficient along the length of a partially filled inclined rotating pipe was reported. The experimental results recommended the operation of a partially filled rotating pipe heat transfer equipment in nearly horizontal configuration to produce the maximum heat transfer within the experimental domain of this study.

The PICOlog6 J-type thermocouples (exposed wire, polytetrafluoroethylene (PTFE) insulated) with a tip diameter of 1.5 mm and a tip temperature range between −270 and 1820 °C were used to measure the temperature (Figure 2a,b). Discrete points were located at the inlet and outlet of the evaporator and condenser physical domain in order to quantify the performances of the heat pipe system at specific measurement locations. The thermocouple points were located 0.248 m into the evaporator (J6 and J7) from the origin and

0.496 m (J3 and J5) in the heat pipe condenser section (X-direction), spaced 0.009 m apart, and was kept constant in the Y- and Z-directions. The liquid fill ratio was constant at 65%, with a total volume of 59 mL.

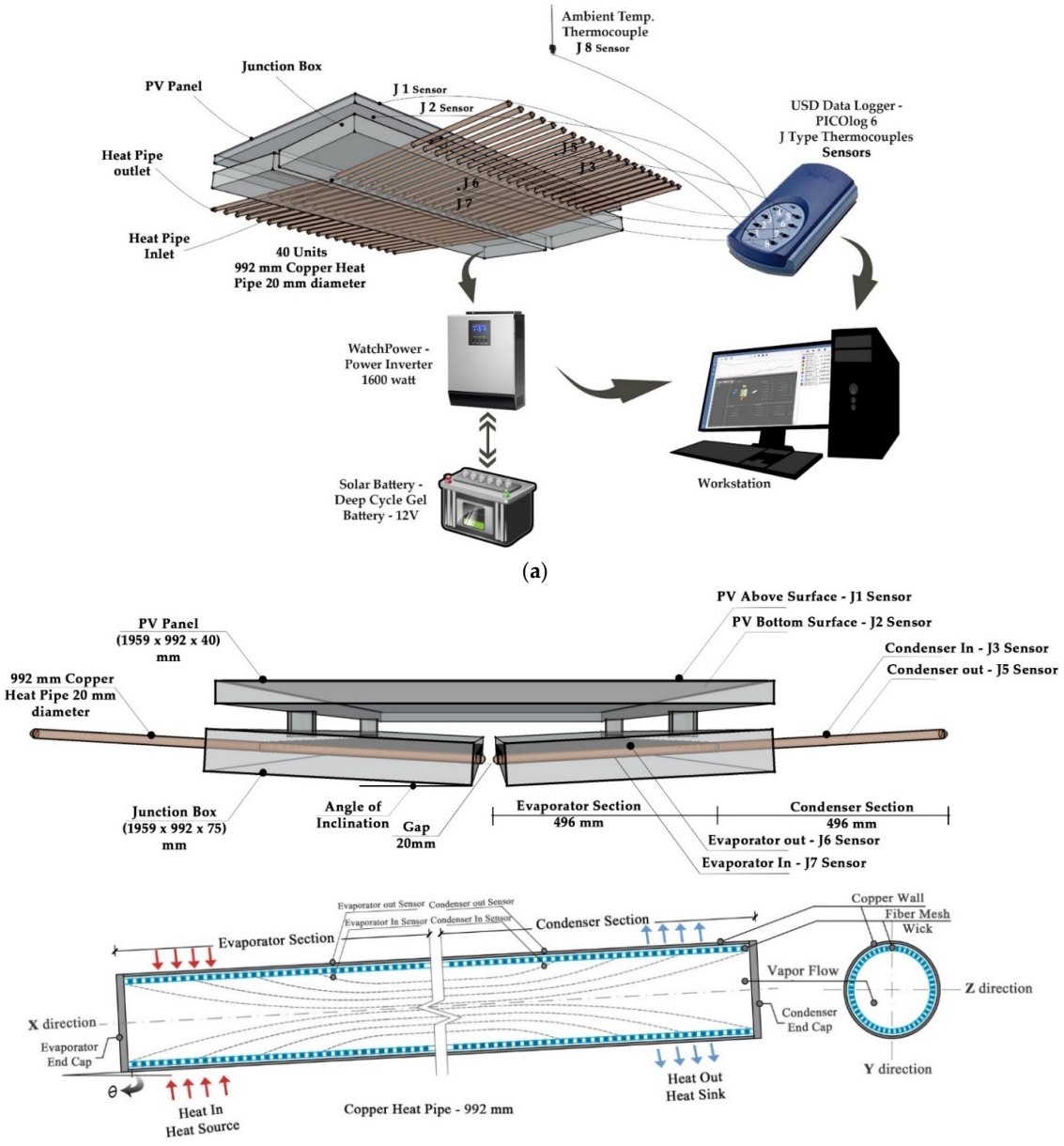

Figure 2. (**a**) Schematic diagram of the experimental setup of PV-HPHE with spanwise 50 mm spacings in the middle arrangement. (**b**) PV-HPHE with spanwise 50 mm spacings in the middle arrangement (above) and the HPHE cross-section (bottom). A baseline experiment was done from August 1 to 12, 2020, to determine the power performance efficiency of the PV-HPHE installed on site, as shown in Figure 3a,b. Two sets of PV panels were installed on site. The first PV panel was installed using 2 thermocouple sensors on the top and bottom surfaces to monitor the temperature and the power generation. The second PV panel was installed in the HPHE parallel to the bottom surface, with 2 thermocouple sensors on the top and bottom surfaces to monitor the temperature and the power generation similarly to what is shown in Figure 2a,b, where the results presented in Tables 5 and 6. The first PV panel served as an independent apparatus to monitor the baseline data of the power generation. The second PV-HPHE panel was the controlled apparatus and was used to investigate how the power generation efficiency was affected by the variables of the HPHE angle of inclination set at 6° and using a 65% refrigerant fill ratio (FR) in the evaporator section.

(**a**)

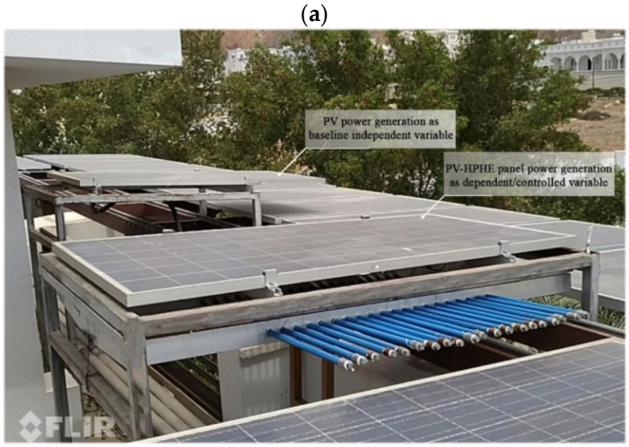

(**b**)

Figure 3. (**a**) Determination of the power performance efficiency of the PV-HPHE that was installed in the Ecohouse, University of Technology and Applied Sciences, Muscat, Oman. (**b**) Physical site of the solar photovoltaic panel installation with heat pipe heat exchanger.

3.3. Experimental Uncertainties

The experimental uncertainties of parameters were calculated using the standard uncertainty equation [34]. The significance of the value of uncertainty established the boundary limitations of the variables of the PV-HPHE under investigation. The standard uncertainties of different parameters that were used in the experimental measurement are shown in Table 2.

Table 2. Experimental uncertainties.

Parameter.	Standard Uncertainty		
	Average	Standard Deviation	Standard Error
Mean bulk temperature (°C)	33.137	0.940	0.355
Mass flow rate (kg/s)	2.057×10^{-5}	6.467×10^{-7}	2.444×10^{-7}
Heat flow (W)	0.791	0.024	0.011
Heat transfer coefficient (W/m^2 K)	2.346	0.015	0.006
Reynolds number Re	1.534	0.078	0.030
Nusselt number Nu	0.936	0.006	0.002
Rayleigh number Ra	1.112×10^{9}	6.518×10^{7}	2.464×10^{7}
Prandtl number Pr	5.014	0.107	0.040
Grashof number Gr	2.220×10^{8}	1.707×10^{7}	6.452×10^{6}
PV-HPHE power generation efficiency	0.289	0.054	0.015
HPHE power generation (W) (Equation (25))	18.577	1.599	0.604
HPHE thermal performance	0.761	0.008	0.003

4. Results and Discussion

Using the data shown in Table 3, the relationship of ambient temperature with the HPHE heat flow generation was calculated using the mean temperature Tb [25] and the logarithmic temperature ΔT_m [26]. The resulting uniform characteristics and consistent proportionality of each heat flow that was derived from the mean and logarithmic temperatures, respectively, are presented in Figure 4. The actual heat transfer coefficient varied from 2.31 to 2.36 W/m^2 K and was inversely proportional to both the HPHE heat flow that was calculated using the mean liquid bulk temperature Tb and the mean logarithmic temperature ΔTm, as shown in Figure 4.

Table 3. HPHE Heat flow generated from convective heat transfer coefficient.

Date	Tilt Angle	Fill Ratio	Ambient Temp.	Overall HTC	Total Cross-Sectional Area	Change in HPHE Internal Temperature Tb (°C)		HPHE Mean Bulk Temperature, (Chatterjee et al., 2018)	Calculated HPHE Heat Flow, (Chatterjee et al., 2018)	HPHE Logarithmic Internal Temperature (Sinnott and Towler, 2020)	Calculated HPHE Heat Flow (Sinnott and Towler, 2020)	Thermal Performance of HPHE
		(%)	(°C)	h	A (m^2)	$T_{E,in}$	$T_{C,in}$	Tb (°C)	Q (W)	Logarithmic ΔTm (°C)	Q (W)	ε = q_{actual}/q_{max}
14/09/20			36.08	2.313	0.01018	28.74	37.69	33.21	0.782	33.01	0.777	74.44%
16/09/20			35.69	2.346	0.01018	28.06	37.20	32.63	0.779	32.41	0.774	76.40%
17/09/20			35.91	2.347	0.01018	28.32	37.50	32.91	0.786	32.70	0.781	76.31%
18/09/20	3°	65	35.32	2.347	0.01018	27.68	36.92	32.30	0.772	32.08	0.766	76.27%
19/09/20			35.36	2.357	0.01018	27.65	36.99	32.32	0.775	32.09	0.770	76.71%
20/09/20			36.58	2.356	0.01018	28.94	38.28	33.61	0.806	33.39	0.801	76.37%
21/09/20			37.83	2.354	0.01018	30.38	39.58	34.98	0.838	34.78	0.833	76.29%

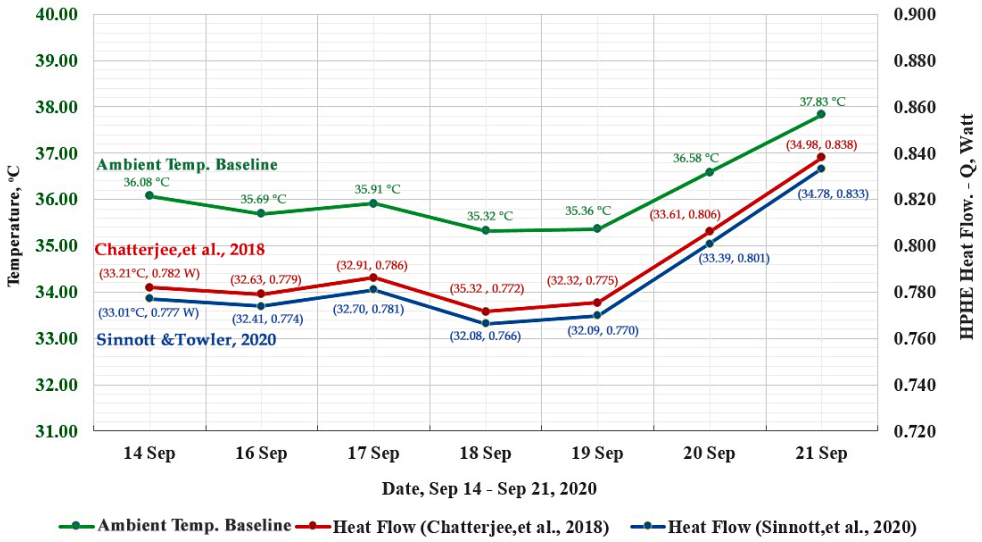

Figure 4. Relationship between the ambient temperature and the HPHE heat flow generation from the mean temperature Tb (Chatterjee et al.) and logarithmic temperature ΔTm (Sinnot et al.).

The mean heat transfer coefficient of 2.34 W/m^2 K was calculated and used to determine the mean heat flow of the HPHE, as shown in Figure 5. The effect between the mean convective heat transfer coefficient and the HPHE heat flow that was generated using the mean bulk liquid temperature Tb showed uniform characteristics when related to the ambient temperature as the baseline. The mean HTC was used to calculate the mean HPHE heat flow and a comparison between the actual HTC was used to calculate the actual HPHE heat flow with both having the bulk temperature Tb, as shown in Figures 6 and 7, using the ambient temperature as the baseline. The result showed an approximate proportionality of the mean and actual HPHE heat flows with the variation in the ambient temperature.

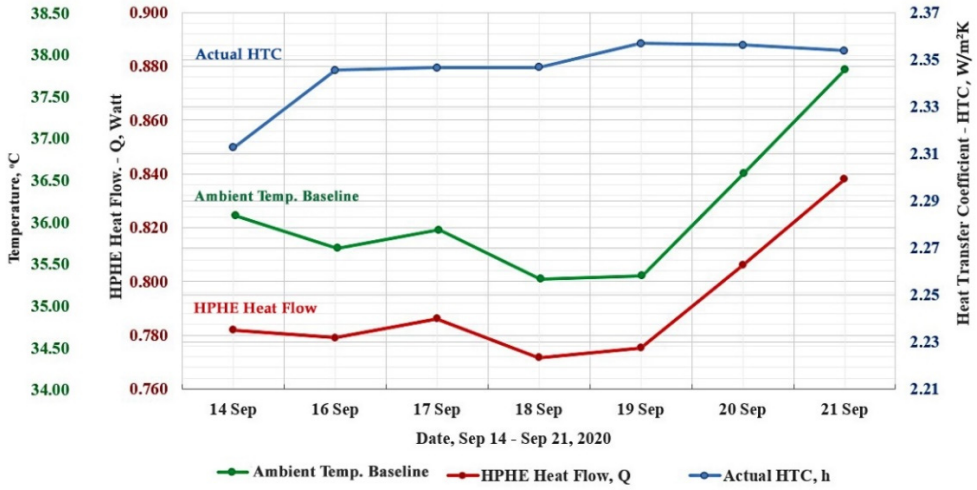

Figure 5. Effect of the actual convective heat transfer coefficient on the HPHE heat flow from Tb using the ambient temperature as the baseline.

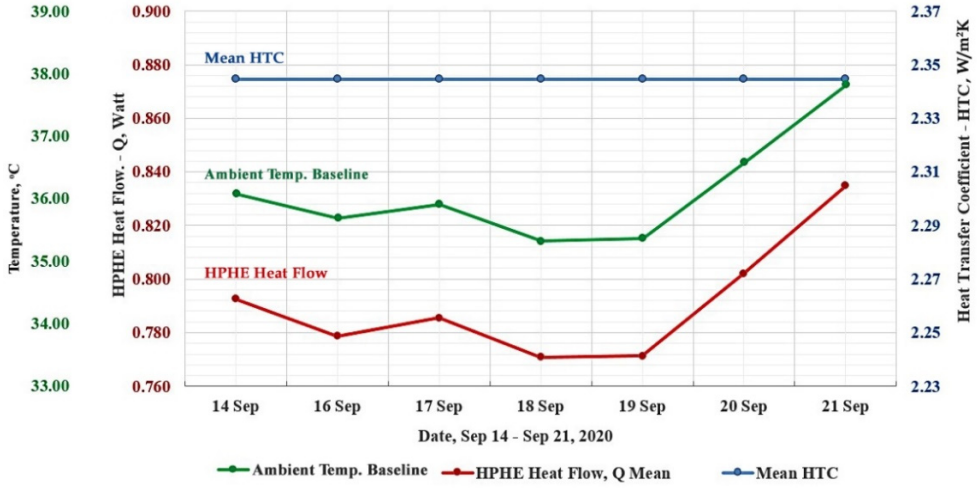

Figure 6. Effect of the mean convective heat transfer coefficient applied to the mean HPHE heat flow from Tb using the ambient temperature as the baseline.

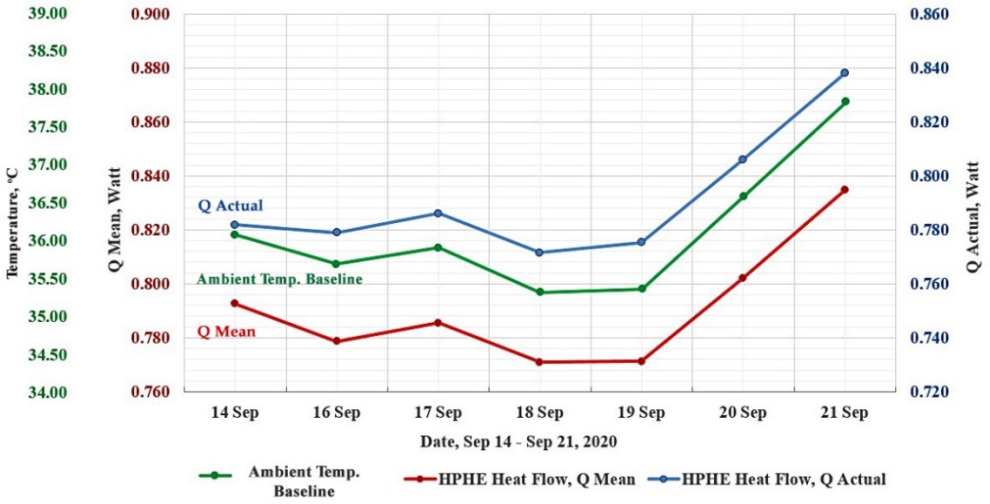

Figure 7. Comparison of the mean h used in the HPHE heat flow and the actual h used in the HPHE heat flow from Tb using the ambient temperature as the baseline.

4.1. Validation of Fluid Dimensionless Numbers

The results of the dimensionless numbers were within the range of the boundary conditions. The Reynolds number of 1.55 was in the range of sub-laminar flow and was very low, which showed the existence of natural (free) convective heat transfer in the HPHE. The dimensionless number that was used as an option in the calculation of natural convection was the Grashof number, whose mean was equal to 2.23×10^8. The mean Prandtl number of 5.0 was greater than air and lesser than water. The product of the Grashof and Prandtl numbers resulted in the mean Rayleigh number of 1.115×10^9, which was the basis of the type of equation to determine the Nusselt number. The Nusselt number is a ratio of the convective to the conductive heat transfer of the liquid. The mean Nusselt number was equal to 0.935, and hence less than 1, which can be interpreted as the HPHE heat transfer of bulk liquid involving less free convection and more conduction, as shown in Table 4.

Table 4. Dimensionless numbers that were based on the local temperature variations.

Date	Mean Bulk Temp	Bulk Temp Diff.	Ts − Tb	Reynold's No.	Prandtl No.	Grashof No.	Rayleigh No.			Nusselt No.	Actual HTC
	Tb (°C)	ΔT (°C)	(°C)	Re	Pr = Cp × μ/k	Gr	Ra/L_{EC}	Ra/D_E	Ra/D_E = Gr × Pr	Nu_{local}	h = k × Nu/L_{EC}
14/09/20	33.21	8.96	2.19	34.654	5.00	2.03×10^8	3.89×10^5	1.02×10^9	1.02×10^9	0.922	2.31
16/09/20	32.63	9.14	2.41	35.852	5.07	2.15×10^8	4.16×10^5	1.09×10^9	1.09×10^9	0.937	2.35
17/09/20	32.91	9.17	2.41	37.092	5.04	2.19×10^8	4.22×10^5	1.10×10^9	1.10×10^9	0.937	2.35
18/09/20	32.30	9.24	2.43	41.296	5.11	2.11×10^8	4.12×10^5	1.08×10^9	1.08×10^9	0.938	2.35
19/09/20	32.32	9.35	2.50	31.668	5.11	2.17×10^8	4.24×10^5	1.11×10^9	1.11×10^9	0.942	2.36
20/09/20	33.61	9.34	2.46	35.124	4.96	2.35×10^8	4.46×10^5	1.17×10^9	1.17×10^9	0.939	2.36
21/09/20	34.98	9.20	2.42	36.251	4.81	2.54×10^8	4.67×10^5	1.22×10^9	1.22×10^9	0.935	2.35

4.2. Effect of Ambient Temperature on the HPHE Thermal Performance

The relationship between the ambient temperature variations and the HPHE thermal performance was analysed. The results showed that that the thermal performance was inversely proportional to the ambient, mean bulk liquid and mean logarithmic temperatures. When the ambient temperature decreased, the HPHE mean bulk liquid and mean logarithmic temperatures also decreased, while the thermal performance increased, as shown in Figure 8.

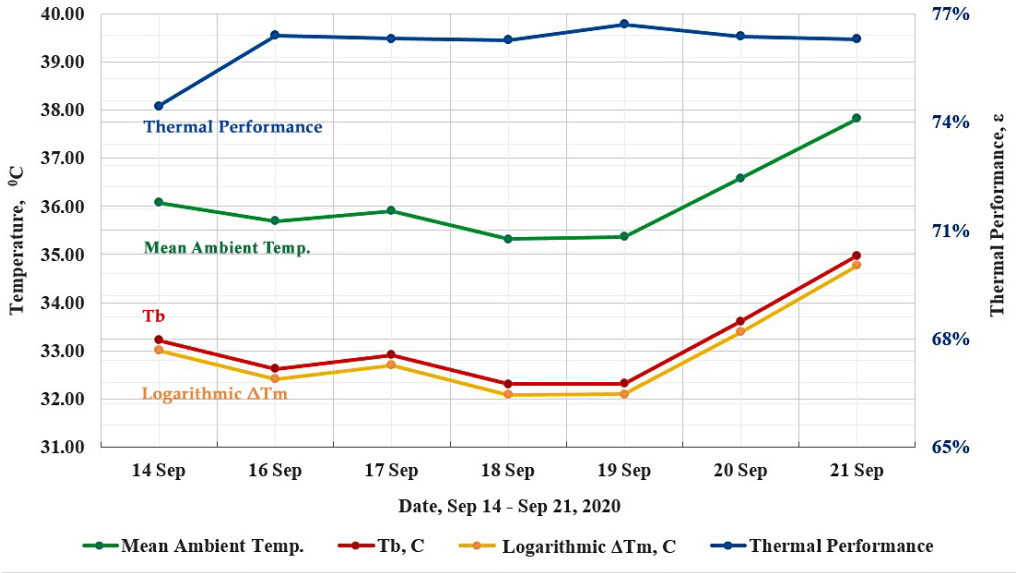

Figure 8. Relationship between the ambient temperature the HPHE thermal performance.

4.3. Effect of HPHE Heat Flow on the PV-HPHE Power Generation Capacity

To test the power generation efficiency that was contributed by the HPHE in the experimental setup to be compared to the thermal performance and heat flow generation, the experimental data results recorded on site from 1 to 12 August 2020 were utilised. This was the period when the apparatus had not experienced operational interference and had achieved continuous data recording. The data were derived from a similar setup of experimental apparatus composed of a separate PV panel as the independent variable, which was compared to the PV-HPHE as the dependent variable. Seven thermocouples were installed on the top and bottom surfaces of both PV and PV-HPHE, two on the external surfaces of the evaporator and condenser of the HPHE and the last was used to monitor the ambient temperature.

The experimental setup had a fill ratio of 65% and an angle of inclination of 3°. The solar irradiation was 911.11 W/m^2 (Al Mabsali et al) [2]. The power capacity was taken within the time frame of 10 a.m.–2 p.m. This was when the solar orientation was approximately perpendicular to the surface of the PV panel. The maximum PV-HPHE power generation was selected from a 15min interval data recording every hour. Using Equations (22)–(25), the results of the experimental setup are shown in Tables 5 and 6, showing a mean PV-HPHE vs. PV power performance efficiency of 29%.

Table 5. Experimental observation of the PV-HPHE panel characteristics.

Date	Tilt Angle	Fill Ratio	Ambient Temp.	NOCT	Ave. Solar Irradiation S	Pico Log Temp. Readings between 10:00–14:00 h (°C)		PV Cell Temp.	Actual Panel Power Production
		(%)	(°C)	(°C)	(W/m^2)	Top	Bottom	(°C)	(W)
01 August 2020	3°	65	28.98	32.15	911.11	32.15	32.83	42.81	70.50
02 August 2020			29.08	32.15	911.11	32.15	33.08	42.91	70.44
03 August 2020			29.32	32.27	911.11	32.27	33.03	43.29	71.13
04 August 2020			31.25	34.10	911.11	34.10	34.73	47.30	71.25
05 August 2020			31.23	33.86	911.11	33.86	34.66	47.01	70.81
06 August 2020			31.08	33.64	911.11	33.64	34.26	46.61	71.38
07 August 2020			31.12	33.82	911.11	33.82	34.34	46.86	72.06
08 August 2020			30.25	31.16	911.11	31.16	31.28	42.96	72.00
09 August 2020			31.55	33.70	911.11	33.70	33.94	47.15	71.63
10 August 2020			34.06	36.36	911.11	36.36	36.90	52.69	70.63
11 August 2020			33.33	37.06	911.11	37.06	36.67	52.76	80.50
12 August 2020			31.23	35.13	911.11	35.13	34.89	48.46	71.63

Table 6. Experimental observations of the PV panel characteristics.

Date	Ambient Temp. (°C)	NOCT (°C)	Ave. Solar Irradiation S (W/m^2)	Pico Log Temp. Readings between 10:00–14:00 h (°C)		PV Cell Temp.	Actual Panel Power Production	PVHP vs. PV Performance Efficiency
				Top	Bottom	(°C)	(W)	(%)
01 August 2020	28.98	34.16	911.11	34.16	33.59	45.11	53.19	32.55%
02 August 2020	29.08	34.44	911.11	34.44	33.81	45.52	55.31	27.34%
03 August 2020	29.32	34.53	911.11	34.53	33.83	45.86	57.19	24.37%
04 August 2020	31.25	36.38	911.11	36.38	35.63	49.90	56.13	26.95%
05 August 2020	31.23	36.20	911.11	36.20	35.46	49.68	57.88	22.35%
06 August 2020	31.08	35.95	911.11	35.95	35.13	49.24	56.19	27.03%
07 August 2020	31.12	35.97	911.11	35.97	35.02	49.31	56.31	27.97%
08 August 2020	30.25	31.97	911.11	31.97	31.35	43.88	55.94	28.72%
09 August 2020	31.55	35.52	911.11	35.52	34.53	49.23	55.06	30.08%
10 August 2020	34.06	37.99	911.11	37.99	37.73	54.55	56.50	25.00%
11 August 2020	33.33	39.52	911.11	39.52	37.74	55.55	56.19	43.27%
12 August 2020	31.23	37.25	911.11	37.25	35.49	50.88	54.50	31.42%

The experimental data that was taken from 14–21 September 2020, shown in Table 7, was used to determine the HPHE efficiency, where the power baseline data were taken

from a separate observation period, shown in Tables 5 and 6. Using a similar PV-HPHE panel, the results of the HPHE heat flow, thermal performance and the 29% PV-HPHE power capacity performance from Tables 5–7 were plotted, as shown in Figure 9. Most of the PV-HPHE daily results had a direct proportionality to the HPHE heat flow generation and were indirectly proportional to the thermal performance.

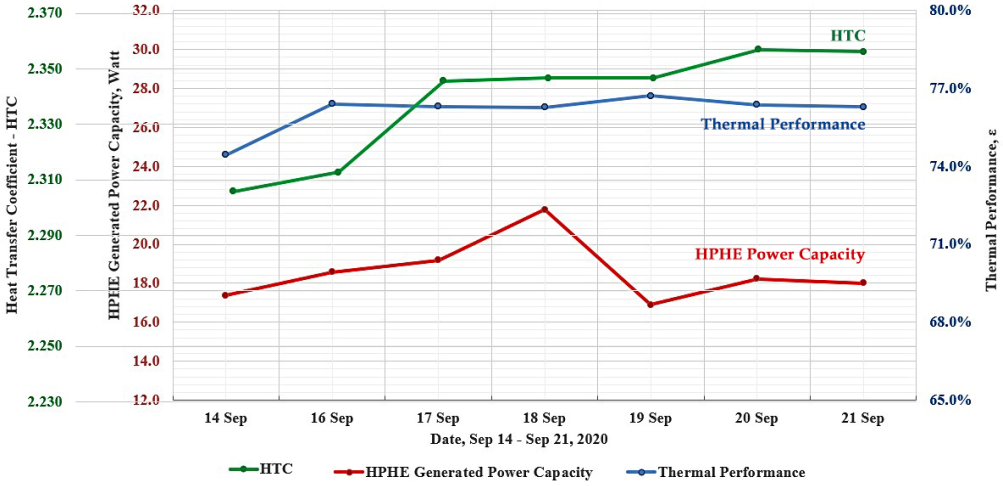

Figure 9. Relationship between the HTC and the HPHE power capacity generation and thermal performance.

Table 7. Experimental observations of the PV-HPHE panel and HPHE from the Picolog data.

Date	Tilt Angle	Fill Ratio	Ambient Temp.	NOCT	Ave. Solar Irradiation S	Picolog Temp. Readings between 10:00–14:00 h (°C)		PV Cell Temp.	Watchpower Ave. PV-HPHE Power Production	Overall HTC	Total Cross-Sectional area	Change in HPHE Internal Temperature Tb (°C)		Calculated PV Power Based on Mean Theoretical Efficiency, Equation (24)	Calculated HPHE Generated Power Based on Mean Theoretical Efficiency, Equation (22)	Calculated HPHE Generated Power Based on Mean Theoretical Efficiency, Equation (25)	Thermal Performance of HPHE
		(%)	(°C)	(°C)	(W/m^2)	Top	Bottom	(°C)	(W)	h	A (m^2)	$T_{E,in}$	$T_{C,in}$	(W)	(W)	(W)	$\varepsilon = q_{actual}/q_{max}$
14/09/20			36.08	37.58	911.11	37.58	37.11	56.11	77.31	2.31	0.01018	28.74	37.69	59.93	17.380	17.38	74.44%
16/09/20			35.69	36.92	911.11	36.92	36.52	54.96	82.63	2.35	0.01018	28.06	37.20	64.05	18.575	18.57	76.40%
17/09/20			35.91	37.14	912.11	37.14	36.77	55.45	85.31	2.35	0.01018	28.32	37.50	66.13	19.179	19.18	76.31%
18/09/20	3°	65	35.32	36.65	913.11	36.65	36.27	54.33	96.88	2.35	0.01018	27.68	36.92	75.10	21.778	21.78	76.27%
19/09/20			35.36	36.78	914.11	36.78	36.39	54.54	75.13	2.36	0.01018	27.65	36.99	58.24	16.889	16.89	76.71%
20/09/20			36.58	37.92	915.11	37.92	37.57	57.08	81.06	2.36	0.01018	28.94	38.28	62.84	18.223	18.22	76.37%
21/09/20			37.83	39.65	916.11	39.65	39.24	60.34	80.13	2.35	0.01018	30.38	39.58	62.11	18.013	18.01	76.29%

5. Conclusions

In this study, HPHE technology was used as a passive PV cooling system to increase its power production capacity so that it is suitable for the hot and arid climate of Oman. This is a novel concept, as heat pipes involving water as a sustainable refrigerant have not been previously tested for cooling purposes in photovoltaic systems to increase their operative performance under harsh climate conditions. Using mathematical principles based on the ambient temperature, mean bulk temperature and mean logarithmic temperature equations, the establishment of the thermal profile of the PV embedded HPHE systems was modelled. The HPHE mean convective heat transfer coefficient of 2.346 W/m^2 K was calculated. Using the ambient temperature as the baseline, approximate results were produced when substituted with the actual HTC values (Figures 6 and 7). The relationship of the ambient temperature with the HPHE heat flow generation from the mean temperature Tb (Chatterjee et al.) and logarithmic temperature ΔTm (Sinnot et al.) showed uniform curve characteristics. The results showed that the dependent variables in HPHE mechanisms that were affected by independent temperature variables are consistent and reliable (Figure 5). The relationship of the mean HTC and actual HTC values applied separately to the heat flow equation using mean bulk temperature showed uniform proportionality with the ambient temperature (Figure 8). The effect of the thermal performance was indirectly proportional to the ambient, mean bulk liquid and mean logarithmic temperatures (Figure 9). The HPHE power capacity was determined from the experimental setup and was used to correlate its effect, which resulted in a high frequency of direct proportionality to the HTC and thermal performance.

In summary, the experimental results showed that the HTC values had a minimal standard error due to the effect of variations in the ambient temperature. The use of the mean HTC of 2.346 W/m^2 K established a specific benchmark that can be used in the succeeding research in this area using PV-HPHE setups.

Author Contributions: Conceptualisation, S.A.A.-M. and H.N.C.; methodology, S.A.A.-M., J.P.C., H.N.C. and M.S.G.; software, S.A.A.-M.; validation, S.A.A.-M. and J.P.C.; formal analysis, S.A.A.-M.; investigation, H.N.C. and M.S.G.; resources, S.A.A.-M.; data curation, S.A.A.-M.; writing—original draft preparation, S.A.A.-M.; writing—review and editing, H.N.C. and M.S.G.; visualisation, S.A.A.-M., J.P.C., H.N.C. and M.S.G.; supervision, H.N.C. and M.S.G.; project administration, H.N.C.; funding acquisition, S.A.A.-M. All authors have read and agreed to the published version of the manuscript.

Funding: This research received no external funding.

Institutional Review Board Statement: The study was conducted according to the guidelines of the Declaration of Helsinki, and approved by the Institutional Review Board of Heriot-Watt University.

Informed Consent Statement: Informed consent was obtained from all subjects involved in the study.

Data Availability Statement: No data reported.

Acknowledgments: The authors would like to thank Heriot-Watt University and the University of Technology and Applied Science Oman for providing the resources to carry out this research.

Conflicts of Interest: The authors declare no conflict of interest.

Nomenclature

Nomenclature	
A	Area (m^2)
Cp	Heat capacity (J/kg K)
D	Inner diameter of pipe (m)
h	Heat transfer coefficient (W/m^2 K)
k	Thermal conductivity (W/m K)
NOCT	Nominal operating cell temperature (°C)

S	Insolation level = 1 kW/m^{2}Ecohouse = 911 W/m^2
v	Kinematic viscosity
$\dot{Q}$	Volume flow rate (m^3/s)
$\dot{m}$	Mass flow rate (kg/s)
q″	Heat flux (W/m^2)
Ft	Correction factor
L	Length (m)
T	Temperature (°C)
ΔT_m	Log mean temperature difference (°C)
q_{actual}	Heat transfer, actual (W)
q_{max}	Heat transfer, ideal (W)
g	Acceleration due to Earth's gravity
Subscript	
Surface	Pipe surface
b	Bulk liquid
w	Local wall
Cell	PV cell
∞	Ambient temperature
Con. in	Condenser in
Evap. in	Evaporator in
e, inlet	Temperature at inlet to evaporator
c, inlet	Temperature at inlet to condenser
e, outlet	Temperature at outlet to evaporator
Greek Symbols	
ε	Thermal performance
μ	Dynamic viscosity (N s/m^2)
ρ	Density (kg/m^3)
ω	Angular velocity (rad/s)
β	Coefficient of thermal expansion
α	Thermal diffusivity
K	Local thermal conductivity (W/m°C)
Non-Dimensional Numbers	
Prandtl number	$Pr = \frac{cp\mu}{k}$
Grashof number	$Gr = \frac{g\ \beta\ (T_s - T_\infty)\ L^3}{v^2}$
Reynolds number	$Re = \frac{\dot{Q}\rho}{\mu D}$
Rayleigh number	$Ra = \frac{g\ \beta\ (T_s - T_b)\ D^3}{v\alpha}$
Nusselt number	$Nu = 0.36 + 0.518\left(\frac{Ra}{\left[1+\left(\frac{0.559}{Pr}\right)^{\frac{9}{16}}\right]^{\frac{16}{9}}}\right)^{\frac{1}{4}}$
Abbreviations	
APSR	Authority for Public Services Regulation
HTC	Heat transfer coefficient
HPHE	Heat pipe heat exchanger
PV	Photovoltaic
PV-HPHE	Photovoltaic heat pipe heat exchanger
UTAS	University of Technology and Applied Sciences

References

1. Authority for Public Services Regulation. *Annual Report*; Authority for Public Services Regulation: Muscat, Oman, 2017.
2. Al-Mabsali, S.; Chaudhry, H.N.; Candido, J. Increasing the passive energy capacity of residential buildings with rooftop photovoltaic modules in hot and arid climates. In *The 1st National Conference on Civil and Architectural Engineering*; Sultan Qaboos University: Muscat, Oman, 2018.
3. Authority for Public Services Regulation. *Annual Report*; Authority for Public Services Regulation: Muscat, Oman, 2018.
4. Authority for Public Services Regulation. *Annual Report*; Authority for Public Services Regulation: Muscat, Oman, 2019.
5. Al-Mabsali, S.A.; Chaudhry, H.N.; Gul, M.S. Numerical Investigation on Heat Pipe Spanwise Spacing to Determine Optimum Configuration for Passive Cooling of Photovoltaic Panels. *Energies* **2019**, *12*, 4635. [CrossRef]

6. Abram, D.; Zachary, R. Conjugate Problems in Convective Heat Transfer: Review. *Math. Probl. Eng.* **2009**, *2009*, 927350.
7. Churchill, S.W.; Chu, H.H. Correlating equations for laminar and turbulent free convection from a horizontal cylinder. *Int. J. Heat Mass Transf.* **1975**, *18*, 1049–1053. [CrossRef]
8. Chaudhry, H.N.; Hughes, B.R.; Ghani, S.A. A review of heat pipe systems for heat recovery and renewable energy applica-tions. *Renew. Sustain. Energy Rev.* **2012**, *16*, 2249–2259. [CrossRef]
9. Chato, J.C. Laminar Condensation Inside Horizontal and Inclined Tubes. Ph.D. Thesis, Massachusetts Institute of Technology, Cambridge, MA, USA, 1960.
10. Mosyak, A.; Hetsroni, G. Analysis of dryout in horizontal and inclined tubes. *Int. J. Multiph. Flow* **1999**, *25*, 1521–1543. [CrossRef]
11. Hetsroni, G.; Yi, J.H.; Hu, B.G.; Mosyak, A.; Yarin, L.P.; Ziskind, G. Heat transfer in intermittent air–water flows—Part II: Upward inclined tube. *Int. J. Mul-Tiphase Flow* **1998**, *24*, 189–212. [CrossRef]
12. Louahlia-Gualous, H.; Le Masson, S.; Chahed, A. An experimental study of evaporation and condensation heat transfer coefficients for looped thermosyphon. *Appl. Therm. Eng.* **2017**, *110*, 931–940. [CrossRef]
13. Kruzhilin, G. Free-convection transfer of heat from a horizontal plate and boiling liquid. *Dokl. AN SSSR (Rep. USSR Acad. Sci.)* **1947**, *58*, 1657–1660.
14. Wang, W.-W.W.; Radcliff, T.D.; Christensen, R.N. A condensation heat transfer correlation for millimeter-scale tubing with flow regime transition. *Exp. Therm. Fluid Sci.* **2002**, *26*, 473–485. [CrossRef]
15. Koyama, S.; Kuwahara, K.; Nakashita, K. Condensation of refrigerant in a multi-port channel. In Proceedings of the International Conference on Microchannels and Minichannels, Rochester, NY, USA, 24–25 April 2003; Available online: https://asmedigitalcollection.asme.org/ICNMM/proceedings-abstract/ICMM2003/36673/193/292032 (accessed on 1 January 2021).
16. Yasuo, M.; Kozo, F.; Shinobu, T.; Masakuni, N. Forced convective heat transfer in uniformly heated horizontal tubes 1st report—Experimental study on the effect of buoyancy. *Int. J. Heat Mass Transf.* **1966**, *9*, 453–463. [CrossRef]
17. Mohammed, H.A.; Salman, Y.K. The effects of different entrance sections lengths and heating on free and forced convective heat transfer inside a horizontal circular tube. *Int. Commun. Heat Mass Transf.* **2007**, *34*, 769–784. [CrossRef]
18. Papoutsakis, E.; Ramkrishna, D.; Lim, H.C. The extended Graetz problem with prescribed wall flux. *AIChE J.* **1980**, *26*, 779–787. [CrossRef]
19. Colle, S. The extended Graetz problem with arbitrary boundary conditions in an axially heat conducting tube. *Flow Turbul. Combust.* **1988**, *45*, 33–51. [CrossRef]
20. Warrington, R.; Powe, R. The transfer of heat by natural convection between bodies and their enclosures. *Int. J. Heat Mass Transf.* **1985**, *28*, 319–330. [CrossRef]
21. Wang, L.; Huang, C.; Hu, J.; Shi, B.; Chai, Z. Effects of temperature-dependent viscosity on natural convection in a porous cavity with a circular cylinder under local thermal non-equilibrium condition. *Int. J. Therm. Sci.* **2020**, *159*, 106570. [CrossRef]
22. Seiichi, N.; Takuro, O. Heat transfer from a horizontal circular wire at small reynolds and grashof numbers—II: Mixed convection. *Int. J. Heat Mass Transf.* **1975**, *18*, 397–413. [CrossRef]
23. Forsberg, C.H. Chapter 7—Natural (free) convection. In *Heat Transfer Principles and Applications*; Forsberg, C.H., Ed.; Academic Press: Cambridge, UK, 2021; pp. 267–304.
24. Davidzon, M.I. Newton's law of cooling and its interpretation. *Int. J. Heat Mass Transf.* **2012**, *55*, 5397–5402. [CrossRef]
25. Chatterjee, S.; Sugilal, G.; Prabhu, S. Impact of inclination on single phase heat transfer in a partially filled rotating pipe. *Int. J. Heat Mass Transf.* **2018**, *123*, 867–878. [CrossRef]
26. Sinnott, R.; Towler, G. Chapter 12—Heat-transfer Equipment. In *Chemical Engineering Design*, 6th ed.; Sinnott, R., Towler, G., Eds.; Butterworth-Heinemann: Oxford, UK, 2020; pp. 773–927.
27. Appendix C: Properties of Water. In *The Shock Absorber Handbook*; Wiley: Hoboken, NJ, USA, 2007; pp. 379–380. Available online: https://www.wiley.com/en-ad/The+Shock+Absorber+Handbook,+2nd+Edition+-p-9780470510209 (accessed on 1 January 2021).
28. Chaudhry, H.N.; Hughes, B.R. Analysis of the thermal cooling capacity of heat pipes under a low Reynolds number flow. *Appl. Therm. Eng.* **2014**, *71*, 559–572. [CrossRef]
29. *Thermophysical Properties of Fluid Systems*; National Institute of Standards and Technology: Gaithersburg, MD, USA, 2016. Available online: https://webbook.nist.gov/chemistry/fluid/ (accessed on 1 January 2021).
30. Andersson, P.; Ross, R.G.; Backstrom, G. Thermal resistivity of ice Ih near the melting point. *J. Phys. C Solid State Phys.* **1980**, *13*, L73–L76. [CrossRef]
31. Saville, D.A.; Churchill, S.W. Laminar free convection in boundary layers near horizontal cylinders and vertical axisymmetric bodies. *J. Fluid Mech.* **1967**, *29*, 391–399. [CrossRef]
32. LeFevre, E.J. *Laminar Free Convection from a Vertical Plane Surface*; National Engineering Laboratory, Heat Division: USA, 1956; Available online: https://books.google.ae/books/about/Laminar_Free_Convection_from_a_Vertical.html?id=cS8ryAEACAAJ&redir_esc=y (accessed on 1 January 2021).
33. Alammar, A.; Al-Dadah, R.K.; Mahmoud, S.M. Effect of inclination angle and fill ratio on geyser boiling phenomena in a two-phase closed thermosiphon—Experimental investigation. *Energy Convers. Manag.* **2018**, *156*, 150–166. [CrossRef]
34. Navidi, W.C. *Statistics for Engineers and Scientists*; McGraw Hill: New York, NY, USA, 2008.